RANS-BASED CFD PREDICTION OF THE HYDRODYNAMIC COEFFICIENTS OF DARPA SUBOFF GEOMETRY IN STRAIGHT-LINE AND ROTATING ARM MANOEUVRES

(DOI No: 10.3940/rina.ijme.2015.a1.308)

Z Q Leong, D Ranmuthugala, I Penesis and **H D Nguyen,** Australian Maritime College, Tasmania

SUMMARY

Computational Fluid Dynamics (CFD) simulations using Reynolds Averaged Navier-Stokes (RANS) equations are increasingly adopted as an analysis tool to predict the hydrodynamic coefficients of underwater vehicles. These simulations have shown to offer both a high degree of accuracy comparable to experimental methods and a greatly reduced computational cost compared to Large Eddy Simulation (LES) and Direct Numerical Simulation (DNS). However, one of the major challenges faced with CFD simulations is that the results can vary greatly depending on the numerical model settings. This paper uses the DARPA SUBOFF hull form undergoing straight-line and rotating arm manoeuvres at different drift angles to analyse the hydrodynamic forces and moments on the vehicle against experimental data, showing that the selection of the boundary conditions and turbulence models, and the quality of the mesh model can have a considerable and independent effect on the computational results. Comparison between the Baseline Reynolds Stress Model (BSLRSM) and Shear Stress Transport with Curvature Correction (SSTCC) were carried out for both manoeuvres, showing that with a sufficiently fine mesh, appropriate mesh treatment, and simulation conditions matching the experiments; the BSLRSM predictions offer good agreement with experimental measurements, while the SSTCC predictions are agreeable with the longitudinal force but fall outside the experimental uncertainty for both the lateral force and yawing moment.

NOMENCLATURE

A_S	Surface area (m^2)
CB	Centre of buoyancy (m)
D	Diameter (m)
L	Overall length (m)
L_S	Surface length (m)
N	Yawing moment (Nm)
N'	Yawing moment coefficient (-); $N/(0.5\rho U^2 L^3)$
P	Rotation origin (-)
R	Turning radius (m)
Re	Reynolds number (-)
u_*	Friction velocity ($m^2\ s^{-1}$)
U	Velocity of body centre of buoyancy relative to fluid ($m\ s^{-1}$)
V_x	Linear velocity as a function of x ($m\ s^{-1}$)
X	Longitudinal force (N)
X'	Longitudinal force coefficient (-); $X/(0.5\rho U^2 L^2)$
y_{wall}	Wall distance (m)
Y	Lateral force (N)
Y'	Lateral force coefficient; $Y/(0.5\rho U^2 L^2)$
y^+	Non-dimensional wall distance (-); $(u_* y_{wall})/\nu$
x,y,z	Cartesian coordinates in the x,y,z-direction (m)
β	Drift angle (°)
ρ	Fluid density ($kg\ m^{-3}$)
μ	Fluid dynamic viscosity ($kg\ m^{-1}\ s^{-1}$)
ν	Fluid kinematic viscosity ($m^2\ s^{-1}$); μ/ρ
∇	Volume (m^3)
r'	Non-dimensional rotation rate (-)
r	Rotational velocity ($rad\ s^{-1}$)

1. INTRODUCTION

The Australian Maritime College (AMC) is exploring both design and operational challenges associated with multiple underwater vehicles operating in proximity. When the vehicles are operating close to each other, their respective wake and pressure fields can adversely interact with one another. These interactions can result in uncontrollable motions of the vehicles, which in extreme cases can lead to mission failure; either due to the inability to maintain a desired trajectory or due to damage arising from collision. Therefore, it is essential to have a good understanding of the interaction behaviour, in order to develop adequate control systems that can deal with these adverse interaction effects. It is also important to identify suitable operating envelopes for the vehicles, enabling them to operate and manoeuvre safely and effectively in close proximity.

With the ongoing development of high performance computing facilities and numerical codes to predict fluid flow and pressure fields in the recent decade, computer-based simulation using Computational Fluid Dynamics (CFD) is slowly gaining acceptance as a reliable analysis tool in underwater vehicle design. Reynolds Averaged Navier-Stokes (RANS)-based CFD simulations have shown to be capable of predicting the hydrodynamic coefficients of underwater vehicles with a high degree of accuracy, comparable to experimental methods [7, 10, 13, 14, 16, 19]; while offering a greatly reduced computational cost in comparison to Large Eddy Simulation (LES) and Direct Numerical Simulation (DNS) due to the lesser mesh requirement to capture the boundary layers on the vehicles [1]. This makes RANS-based simulations attractive to investigate the hydrodynamic interaction between multiple underwater vehicles by simulating conditions that are difficult or costly to achieve through experimental means, e.g. full scale tests, free running vehicles, and flow visualisation. However, one of the major challenges faced when using CFD as an analysis tool for hydrodynamics is that the computational results can vary greatly depending on the

experience of the analyst, the settings utilised such as the boundary condition and the turbulence models, and the quality of the mesh model; thus necessitating validation through experimental or full scale data.

A review by the authors on RANS-based CFD studies on the hydrodynamics of the Defense Advanced Research Projects Agency (DARPA) SUBOFF submarine geometry (see Figure 1) revealed a high degree of variation in the selection of turbulence models, and which turbulence model gives the most accurate prediction compared to experimental data. Given the large number of studies, the following discussion focuses only on RANS-based CFD studies in the recent decade related to the SUBOFF geometry, that include validation against experimental data (see Table 1). The SUBOFF was considered for the review as it has been an internationally accepted benchmark model for validating both CFD and experimental testing methods. The application of interest is the prediction of the forces and moments acting on the SUBOFF undergoing either straight-line or rotating arm manoeuvres at different drift angles.

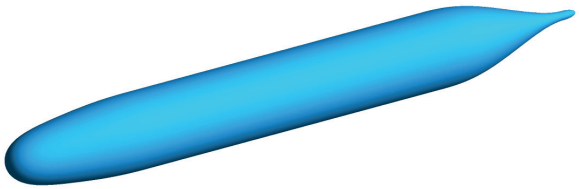

Figure 1: DARPA SUBOFF unappended hull geometry.

From the review, the Reynolds Stress Models (RSM) were found to outperform the other RANS-based turbulence models in predicting the hydrodynamic forces and moments acting on the SUBOFF geometry. The RSM predictions from the studies by Phillips et al. [10], Toxopeus et al. [14], and Watt et al. [16] were generally found to be within 10% of the experimental results at the highest drift angle investigated, followed by Shear Stress Transport (SST) model predictions which were within 25%. Although the other turbulence models performed well at a drift angle of zero degrees against experimental measurements, the agreement quickly depreciated as the drift angle increased. The SST model was found superior to other turbulence models in studies where RSM was not investigated, with predictions also within 25% of the experimental measurements [7, 15].

The exceptions to the above findings were Marshallsay & Eriksson [8] and Zeng & Zhu [18]. The results of their studies showed that the predictions from the Spalart-Allmaras (SA) and k-ω models respectively outperformed the SST model when compared against experimental measurements. However, caution needs to be exercised before applying these results as the SST model is a more comprehensive turbulence model compared to SA and k-ω models and should perform better in terms of accuracy, requiring only longer computational time compared to the other two turbulence models on the same mesh domain [9]. It is therefore hypothesised that the discrepancy in turbulence model performance is due to a combination of the following modelling factors: inappropriate application of y^+ in the near-wall mesh for the selected turbulence model; under-prescribing the total thickness of the inflation layers compared to the boundary layer thickness of the SUBOFF geometry; and/or non-matching dimensions between the numerical tank and experimental tank domains, thus not accounting for blockage and boundary effects.

This paper examines the ability of CFD to reproduce the experimentally measured forces and moments acting on the unappended SUBOFF undergoing steady straight-line and rotating arm manoeuvres at different drift angles. The study utilised the Shear Stress Transport with Curvature Correction (SSTCC) model and Baseline Reynolds Stress Model (BSLRSM) as they are the two most advanced and comprehensive RANS-based turbulence models thus far. Previous work at AMC by the authors on the CFD modelling of underwater vehicles utilising different settings including different turbulence models [2, 3] has showed that the SST model consistently generate predictions that are closer in agreement with experimental data. This includes the

Table 1: List of related CFD simulation studies of the SUBOFF geometry

Author(s)	Turbulence Models	Test Case(s)	SUBOFF Configuration(s)
Kim et al. [7]	k-ω; Shear Stress Transport (SST)	Rotating arm	Unappended; appended with sail
Marshallsay & Eriksson [8]	SA; k-ε; k-ω; SST	Straight-line, rotating arm	Unappended (rotating arm), appended with sail and stern planes (straight-line)
Phillips & Turnock [10]	Spalart-Allmaras (SA); k-ε; k-ω; SST; Sperziale, Sarker and Gatski Reynolds Stress Model (SSGRSM)	Straight-line	Unappended;
Toxopeus et al. [14]	k-ω; SST; Baseline Reynolds Stress Model (BSLRSM)	Rotating arm	Unappended;
Vaz et al. [15]	SA; SST	Straight-line	Appended with sail and stern planes
Watt et al. [16]	SA; k-ε; Re-Normalised Group (RNG) k-ε; k-ω; Baseline k-ω; SST; BSLRSM	Straight-line	Unappended
Zeng & Zhu [18]	k-ε; RNG k-ε; Realizable k-ε; k-ω; SST	Straight-line	Appended with stern planes

hydrodynamic forces, moments, pressure distribution, and friction distribution along the vehicle. This paper does not attempt to provide an exhaustive analysis of the ability of the turbulence models to represent the flow physics; rather, it explores the effects of the previously mentioned modelling factors on the force and moment predictions, i.e. application of y^+ in the near-wall mesh, total thickness of the inflation layers, and model boundary conditions. The focus is based on the argument that the effects of the modelling factors on the predictions need to be established and minimised if possible, and the CFD model settings has to correctly represent the experimental conditions before validation of the CFD results can be addressed. This area has been surprisingly neglected as the majority of CFD studies on the SUBOFF geometry have focused on methodologies to validate the CFD predictions with very limited discussion on the factors that can affect the predictions. The authors anticipate the developed CFD methodology from modelling the SUBOFF geometry in this paper to be a starting point for the upcoming, more sophisticated simulation models of multiple underwater vehicles in close proximity.

2. GEOMETRY MODEL AND NON-DIMENSIONLISATION OF RESULTS

The axisymmetric unappended SUBOFF model used in this study is defined by the geometric equations provided by Groves et al. [6], with the computer model created with an accuracy of 0.001m. The unappended SUBOFF model was selected as there is limited experimental data for the appended configurations undergoing rotating arm manoeuvres. Table 2 gives the geometric characteristics of the SUBOFF model shown in Figure 2. The overall length of the SUBOFF was used as the characteristic length for the non-dimensionalisation of the hydrodynamic forces and moments, as well as for Reynolds scaling in this report. The equations and notations used are in accordance with the David Taylor Naval Ship Research and Development Center (DTNSRDC) Revised Standard Submarine Equations of Motion [5], unless otherwise noted.

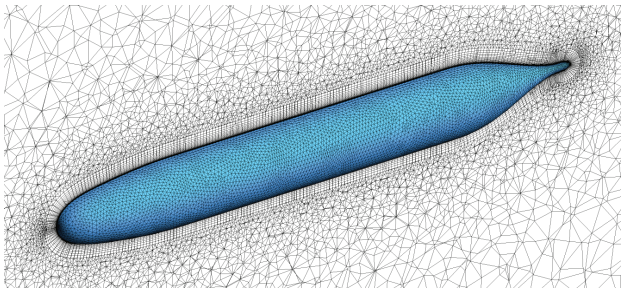

Figure 2: Mesh model of the SUBOFF geometry.

Table 2: Geometric characteristic of the SUBOFF model.

Description	Symbol	Value	Unit
Overall length	L	4.356	[m]
Surface length	L_S	4.489	[m]
Diameter	D	0.508	[m]
Surface area	A_S	5.986	[m^2]
Volume	∇	0.698	[m^3]
Centre of buoyancy	CB	0.461L	[m]

Note: geometric parameters obtained via CFD software.

3. STRAIGHT-LINE MANOEUVRE AT DIFFERENT DRIFT ANGLES

3.1 SIMULATION SETUP

The computational fluid domain was given the same dimensions and test conditions as the David Taylor Research Centre (DTRC) Towing Basin in order to assist with the validation of the CFD results against the experimental data [11]. The numerical towing basin dimensions and testing parameters are given in Table 3.

Table 3: Straight-line manoeuvre test case parameters.

Description	Symbol	Value	Unit
Basin width	-	15.545	[m]
Basin depth	-	6.706	[m]
Model submergence depth	-	3.353	[m]
Towing velocity	U	3.344	[m s^{-1}]
Reynolds Number	Re	1.416×10^7	[-]
Drift angle	β	0 to 18	[°]
Fluid density	ρ	9.983×10^2	[kg m^{-3}]
Fluid dynamic viscosity	μ	1.028×10^{-3}	[kg m^{-1} s^{-1}]

Figure 3 shows the computational fluid domain with the local and global coordinate systems for the straight-line manoeuvre test case, with the SUBOFF hull as a no-slip wall; the top, side and bottom boundaries as free-slip walls; and the boundary behind the SUBOFF as an opening with zero relative pressure. The top, side and bottom boundaries distances to SUBOFF are matched to the experiment dimensions in order to account for blockage and boundary effects that may be present in the experimental data. The remaining boundary in front of the model was defined as an inlet, with a prescribed flow speed of U. The length of the domain was reduced to a distance of 3L forward and 5L aft of the SUBOFF model to reduce the mesh load while ensuring the pressure and wake fields generated by the SUBOFF are sufficiently resolved within the domain.

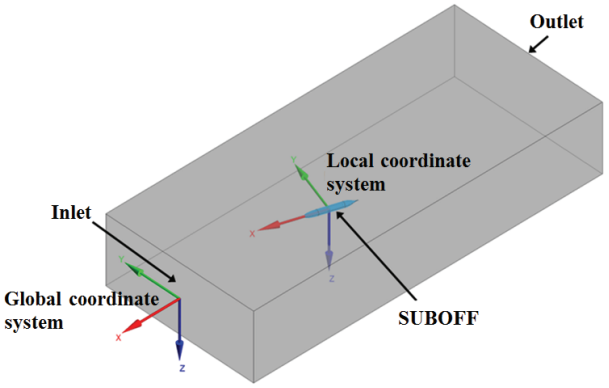

Figure 3: Computational domain and coordinate systems for straight-line manoeuvre.

The simulations were performed with the commercial CFD code ANSYS CFX in steady-state, using the two RANS-based turbulence models Baseline Reynolds Stress Model

(BSLRSM) and Shear Stress Transport with Curvature Correction (SSTCC). The BSLRSM accounts for streamline curvature, rotational flow, and rapid changes in strain rate in a more rigorous manner than the standard SST model at the expense of longer computational time due to the additional equations solved. Compared to the standard SST model, which assumes the eddy-viscosity to be the same in all directions (isotropic), the BSLRSM closes the RANS equations by resolving six additional transport equations for the Reynolds stresses and the dissipation rate, thus offers better accuracy in cases where turbulence is strongly anisotropic.

In the SSTCC model, the standard SST model has been coupled with the Curvature Correction model [12] in order to improve the sensitivity to the turbulence effects caused by the surface curvature of the SUBOFF, i.e. enhanced turbulence at the concave surface of the SUBOFF tail and decreased turbulence at the convex surface of the SUBOFF nose. Thus it was deemed desirable in this study to determine whether the SSTCC model offers predictions comparable to the BSLRSM for the SUBOFF hull form.

3.2 DISCRETISATION STUDY

For the discretisation of the computational domain, an unstructured hybrid tetrahedral mesh approach was used; i.e. triangular prismatic inflation layers around the SUBOFF to capture the boundary layer, and unstructured tetrahedrons in the far field. The selection of the unstructured mesh approach was based on its ability to relatively easily accommodate mesh deformation and automatic re-meshing, features that will be required when future simulation of multiple vehicles in relative motion is carried out. The unstructured mesh approach, although requiring a higher mesh density, has also been established to offer the same degree of accuracy in comparison to a structured mesh [4].

In order to establish the mesh requirements of the turbulence models; the effects of the mesh resolution, total thickness of the inflation layers around the SUBOFF, and the non-dimensional distance y^+ of the first inflation layer off the SUBOFF surface on the predictions of the forces and moments acting on the SUBOFF model were examined. A drift angle of 18° was selected for the discretisation study in congruence with the maximum angle of the experimental data.

3.2 (a) Mesh Independence Study

An initial mesh model was created based on the following criteria: the surface area of the mesh model of the SUBOFF hull was within 0.1% of the geometry model; a maximum domain mesh body size of 1m; a maximum y^+ of 0.5 for the first layer mesh around the SUBOFF; and the minimum total thickness of the inflation layers around the SUBOFF hull matched to 2 times Prandtl's $1/7^{th}$ power law theoretical estimate of turbulent boundary layer thickness over a flat plate, i.e. $2\times0.16L_S/\mathrm{Re}_{L_S}^{1/7}$ [17]. For the latter, the overall surface length L_S was used instead of the overall length L of the vehicle to account for the surface curvature. The surface mesh size on the SUBOFF was selected as the refinement variable for the mesh independence study.

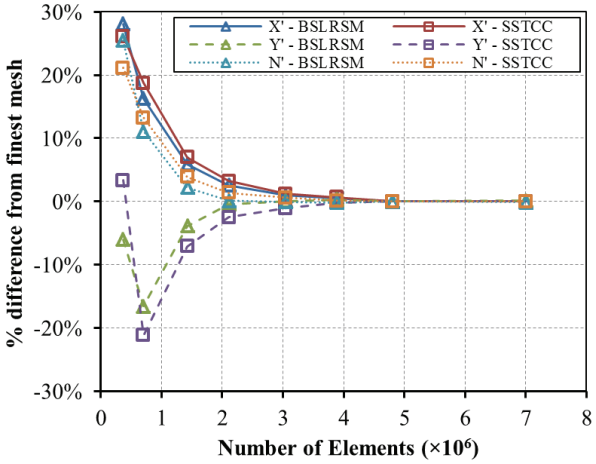

Figure 4: Percentage difference of the longitudinal force coefficient *X'*, lateral force coefficient *Y'*, and yawing moment coefficient *N'* predictions from the finest 7 million elements mesh solution vs number of mesh elements for the SUBOFF straight-line manoeuvre test case at a drift angle of 18°.

Figures 4 shows the percentage difference of the predicted longitudinal force, lateral force and yawing moment from the finest 7 million elements mesh solution as a function of mesh element density for the two turbulence models investigated. It is seen that at about 3.9 million elements, the forces and moment predictions of the two turbulence models were within 0.1% of the finest mesh investigated, thus the discretization error is considered minimal. As a conservative measure, the 4.8 million elements mesh model configuration was used for the remainder of the discretisation study.

3.2 (b) y^+ Study

Figure 5 shows predicted forces and moments on the SUBOFF with respect to the mean y^+ around the hull. Using the solution at y^+=0.5 as the baseline, the force and moment predictions were found consistent (within 1.5%) for y^+ values up to 2 for the both the BSLRSM and SSTCC turbulence models. At $2<y^+\leq10$; the BSLRSM and SSTCC longitudinal force predictions were found to decrease by up to 7.3% and increase by up to 4.4% respectively. The variation in the lateral force and yawing moment predictions were within 2.4% for both turbulence models. This behaviour is attributed to the reduced node resolution within the viscous sub-layer as the y^+ increases, thus reducing the accuracy of the low Reynolds wall treatment model to resolve the boundary layer. At $10<y^+\leq100$, the lateral force predictions were found to decrease considerably as y^+ increases; with differences up to 28.3% for the SSTCC and 20.2% for the BSLRSM at y^+=100. The yawing moment predictions were found to increase as y^+ increases, with differences up to 12.6% for the SSTCC and

8.9% for the BSLRSM at y^+=100. The trends in the longitudinal force predictions with respect to y^+ for both turbulence models were less distinguishable; with differences within 10% for the STTCC and 4.4% for the BSLRSM. The change in trend observed at y^+>10 onwards is due to the switching from the low Reynolds wall treatment model to the empirical-based wall function formulation which occurs at around y^+=10. The gradual increase in the variation of the lateral force and yawing moment predictions as y^+ increases is due the reduced mesh resolution in the portion of the boundary layer closest to the surface. The low mesh resolution reduces the sensitivity of the wall function model, and hence the ability to predict the effects of an adverse pressure gradient on the boundary layer, thus delaying the predicted boundary layer separation.

Based on the above findings, a y^+ of 0.5 was selected for the mesh model to be used in the remaining straight-line simulations in this study. This ensures that the maximum y^+ around the SUBOFF falls well below the conservative value of 1 as the predictions were found to be closely similar under the y^+ threshold of 2 when using the low Re wall treatment model. The wall function model (y^+>10) is deemed insufficiently accurate to predict the forces on the SUBOFF for oblique flows due the large difference in predictions compared to the low Reynolds wall treatment model at y^+ of 0.5 (Figure 5). The low Re wall treatment model should always be viewed as the more accurate solution compared the wall function model as the former resolves the boundary layer down to the sub-viscous layer, which is important to accurately predict adverse pressure gradient and separation within the boundary layer. In cases where the low Reynolds wall treatment with a y^+<1 is unaffordable due to geometric complexity or limitations in computational resource, the wall function with a y^+ near the minimum limit of 11 is recommended as the quality of the lateral force and yawing moment predictions using the wall function depreciates considerably as y^+ increases beyond 20 (Figure 5).

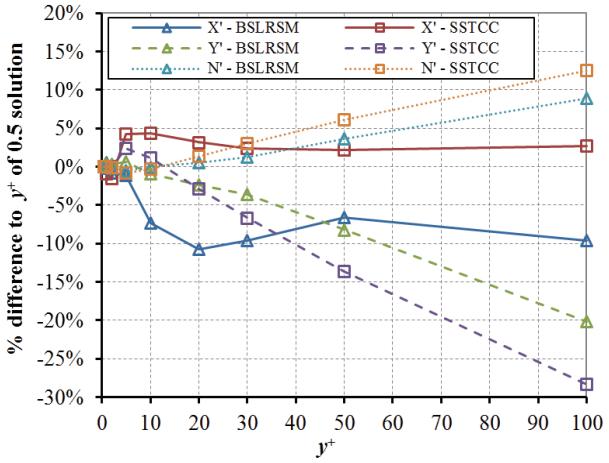

Figure 5: Percentage difference of the longitudinal force coefficient *X'*, lateral force coefficient *Y'* and yawing moment coefficient *N'* predictions as percentage difference from the y^+ of 0.5 solution versus y^+ for the SUBOFF straight-line manoeuvre test case at a drift angle of 18°.

3.2 (c) Thickness of Inflation Layer

The effect of the total thickness of the SUBOFF boundary inflation layers on the predictions is examined using the BSLRSM. Table 4 outlines the four theoretical estimates of the boundary layer thickness to which the total thickness of the inflation layers were matched. The laminar boundary thickness is based on the Prandtl's estimate for laminar flow over a flat plate, $5.00L_S/\mathrm{Re}_{L_S}^{1/2}$; while the turbulent boundary thickness is based on the Prandtl's estimate for turbulent flow, $0.16L_S/\mathrm{Re}_{L_S}^{1/7}$ [17]. The y^+ was maintained at 0.5 throughout the simulations.

Table 4: Theoretical estimates of the boundary layer thickness.

Property	Value	Unit
Laminar layer thickness	5.879×10^{-3}	[m]
Turbulent layer thickness	6.806×10^{-2}	[m]
1.5 × turbulent layer thickness	1.021×10^{-1}	[m]
2 × turbulent layer thickness	1.361×10^{-1}	[m]
3 × turbulent layer thickness	2.042×10^{-1}	[m]

Figure 6 shows predicted forces of the different boundary layer estimates with respect to the mean y^+ around the SUBOFF hull. The laminar estimate resulted in higher longitudinal force, lower lateral force and higher yawing moment predictions compared to the turbulent estimates. It is also seen that there is a degree of total thickness dependency in the predictions with the turbulent estimates. When prescribing a total thickness of 1.5 (and above) times the turbulent estimate, there were no noticeable differences in predictions. The observed behaviour is due to the effective boundary layer has yet recover to the freestream velocity prior to transition from the inflation layers to the much thicker unstructured tetrahedral mesh, thus artificially thickening the predicted boundary layer. As a conservative measure, a total thickness of the inflation layers matching two times the turbulent layer thickness estimate was used for the remainder of the study.

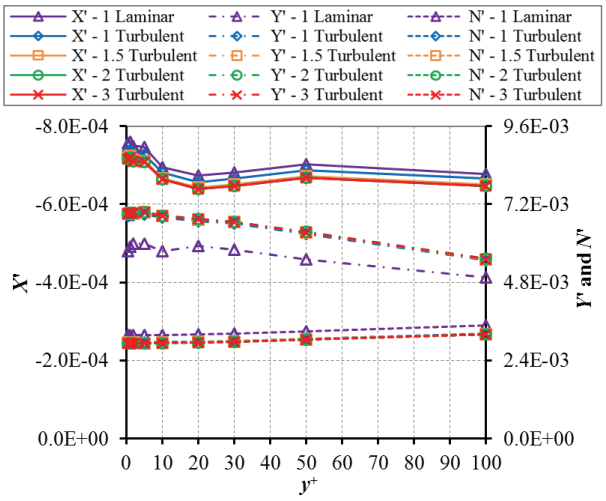

Figure 6: Longitudinal force coefficient *X'*, lateral force coefficient *Y'*, and yawing moment coefficient *N'* predictions of different inflation layer total thickness versus y^+ for the SUBOFF straight-line manoeuvre test case at a drift angle of 18°.

3.3 COMPARISON WITH EXPERIMENTS

Figures 7, 8 and 9 show the predicted longitudinal force, lateral force and yawing moment respectively on the SUBOFF undergoing straight-line manoeuvres at different drift angles in comparison with the experimental data made by Roddy [11]. The experimental data is widely used by researchers to validate their CFD methods [10, 13, 16]. However, there are some limitations in the quality of the experimental data for measurements of low force magnitudes.

A review of the experimental data revealed that the measurements are reliable at drift angles of 10 degrees and below for the longitudinal force, and 8 degrees and above for the lateral force and yawing moment. Figures 7 and 8 show the poor repeatability in the experimental results between the corresponding positive and negative drift angles, with more than 5% variation outside the above range. Thus, validation of the simulation predictions outside the above range is avoided. It is noted that the poor repeatability behaviour occurs when the measured values were roughly less than a force coefficient of 1.000×10^{-3} (i.e. 100N). This behaviour indicates that the resolution of the load cells used in the DTRC towing tank experiment were not sufficient for measurements below 100N. The uncertainty in the measurements was reported to be within 10.0%, although the contribution of the mounting arrangement to the recorded values was not available.

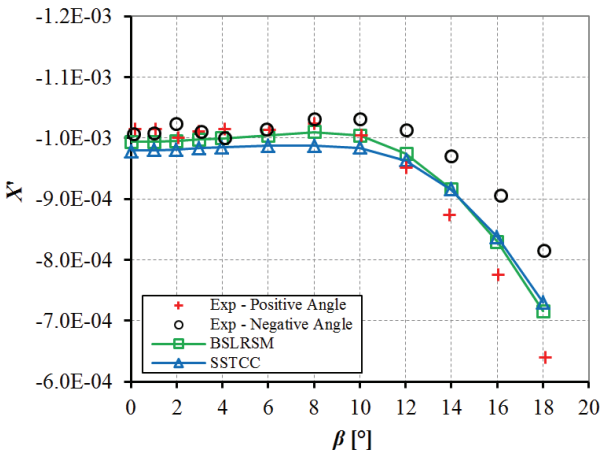

Figure 7: CFD predictions and experimental measurements [11] of the longitudinal force coefficient *X'* versus drift angle β for the SUBOFF straight-line manoeuvre test cases.

The BSLRSM predictions were found to be in good agreement with the experimental positive angle measurements, i.e. within 2.1% for the longitudinal force at drift angles of 10 degrees and below, and 5.0% for the lateral force at 8 degrees and above. The SSTCC longitudinal force predictions were found to be within 5.0% of the experimental positive angle results at the above angles. However, the SSTCC tends to under-predict the lateral force by a maximum of 21.1%, which is well outside the 10.0% experimental uncertainty. This suggests that SSTCC is not suitable to predict the lateral force hydrodynamic coefficients for the SUBOFF hull form at large drift angles. For the yawing moment, the BSLRSM and SSTCC were within 5.1% and 11.0% of the experimental positive angle results respectively at 8 degrees and above.

The findings above indicate that the BSLRSM predicts earlier boundary layer separation, thus producing higher lateral force and yawing moment predictions at angles of attack above 4 degrees compared to the SSTCC model. The BSLRSM computational time was found to be around 20% longer than the SSTCC. Thus, it is within reason to conclude that the accuracy in predictions gained in using the BSLRSM outweighs the extra computational time.

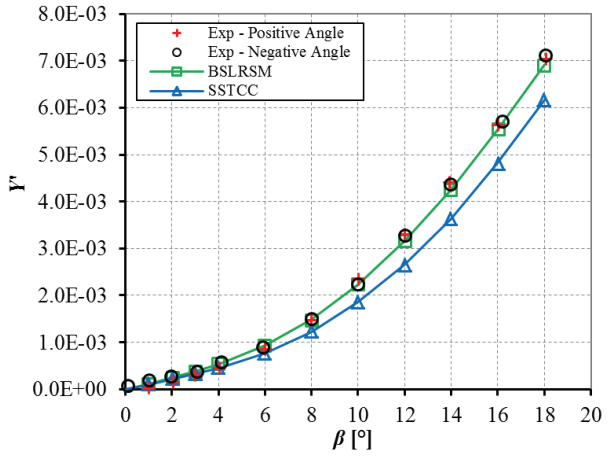

Figure 8: CFD predictions and experimental measurements [11] of the lateral force coefficient *Y'* versus drift angle β for the SUBOFF straight-line manoeuvre test cases.

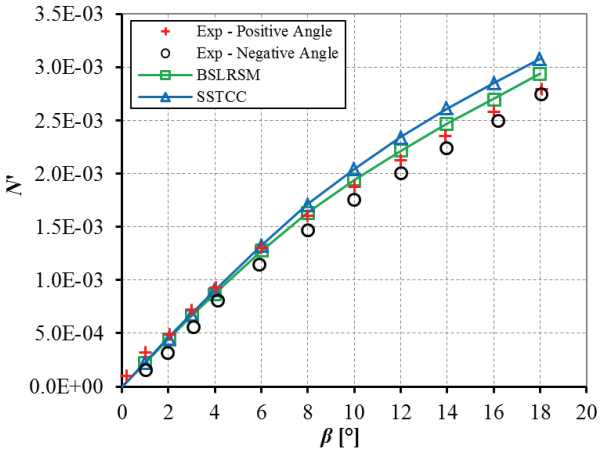

Figure 9: CFD predictions and experimental measurements [11] of the yawing moment *N'* versus drift angle β for the SUBOFF straight-line manoeuvre test cases.

4. ROTATING ARM MANOEUVRE AT DIFFERENT DRIFT ANGLES

Results from the straight-line manoeuvre test cases showed that the BSLRSM was superior to the SSTCC in predicting the longitudinal and lateral forces acting on the SUBOFF at different drift angles when compared to the experimental measurement. However, large variations between the experimental measurements at the certain corresponding positive and negative drift angles limited the validity of the findings. Therefore, the performance of the turbulence models were reviewed under a different flow condition, i.e. with the SUBOFF undergoing a rotating arm manoeuvre at different drift angles, in order to supplement and establish the credibility of the straight-line manoeuvre test case findings.

4.1 SIMULATION SETUP

The computational fluid domain was given the same dimensions and test conditions as Naval Surface Warfare Center Carderock Division (NSWCCD) Rotating Arm Basin in order to assist with the validation of the CFD results against the experimental data [14]. The numerical Rotating Arm Basin dimensions and test conditions matching the experiment are given in Table 5.

Figure 10 illustrates the rotating arm manoeuvre whereby the SUBOFF undergoes a steady yaw rotation. The turning rate is positive for a turn to starboard. The centre of buoyancy *CB* is located at 0.462*L* aft of the nose of the submarine, and was used as the reference point for the forces and moments on the hull. The variable *P* represents the rotation origin and β represents the drift angle. The non-dimensional rotation rate *r'* is defined as,

$$r' = \frac{r \cdot L}{U} = \frac{L}{R} \qquad (1)$$

where *L* is the length overall , *U* is the linear velocity, r is the rotational velocity of *CB* with respect to the origin of the global coordinate system, and *R* is the turning radius of *CB*. The investigated parameters of the SUBOFF rotating arm manoeuvres are outlined in Table 6. For all simulation cases *U* and *r* was fixed at 1.543m s^{-1} and 0.13 rad s^{-1}, respectively.

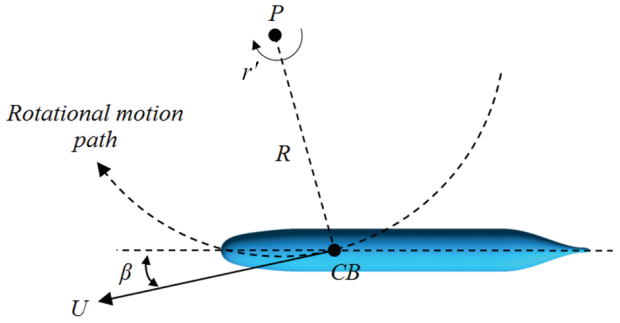

Figure 10: Description of the rotating arm manoeuvre

Table 5: Rotating arm manoeuvre test case conditions

Description	Symbol	Value	Unit
Basin diameter	-	79.2	[m]
Basin depth	-	6.1	[m]
Model submergence depth	-	3.05	[m]
Fluid density	ρ	9.983×10^{2}	[kg m^{-3}]
Fluid dynamic viscosity	μ	1.028×10^{-3}	[kg m^{-1} s^{-1}]

Table 6: Rotating arm manoeuvre test case parameters

Drift Angle, β [°]	Rotation rate, *r'*	Turning Radius, *R* [m]
4	0.3577	12.178
6	0.3598	12.108
8	0.3619	12.038
10	0.3639	11.969
12	0.3660	11.901
14	0.3681	11.833
16	0.3702	11.767
17	0.3712	11.734
18	0.3723	11.701
20	0.3743	11.636

Note: Test parameters obtained from Toxopeus et al [14]

Figure 11 shows the computational domain and coordinate systems for the rotating arm manoeuvre test case. A semicircle domain was used instead of a full circle in order to prevent the SUBOFF from interacting with its own wake. This condition was observed in the experiments whereby the data collection was limited to one revolution of the SUBOFF model. The local coordinate system is shown with its origin located at *CB* of the SUBOFF geometry and the global coordinate system located at centre of the semicircle domain. To simulate the SUBOFF undergoing the rotating arm manoeuvre, the hull was moved in a rotating frame along with the domain at the rotational velocity r as outlined in Table 6. The SUBOFF model was defined as a no-slip wall; the top, inner-ring, outer-ring and bottom boundaries defined as free-slip walls; the outlet defined as an opening with zero relative pressure; and the inlet defined as an inlet with a cylindrical flow velocity. The cylindrical flow velocity V_x is defined as the linear velocity as a function of *x*, i.e. $V_x = rx$.

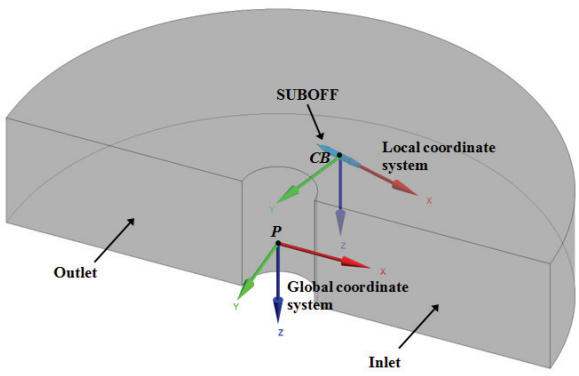

Figure 11: Computational domain and coordinate systems for rotating arm manoeuvre

4.2 VERIFICATION OF THE FLOW WITHIN THE ROTATIONAL DOMAIN

Verification of the rotational flow field in the computational domain was carried out without the SUBOFF model using the settings of the simulation case β = 16° (see Table 6), i.e. the domain rotating at rotational velocity of 1.312×10^{-1} rad s^{-1}. This allows the effects of the boundary conditions on the flow field to be identified without the influence of the SUBOFF model. To establish the accuracy of the flow field, the linear velocity at *CB* (x, y, z = 0, -11.767, 0) was compared to the theoretical solution, i.e. $V = rR$.

It was found that the quality of the flow field in the rotating arm manoeuvre test case was much more sensitive to boundary conditions compared to the straight-line manoeuvre test case. Given that a large number of combinations for the boundary conditions were examined, the following discussion will focus on three selected inlet options closest to replicating the conditions of the experiment. The three options for the inlet boundary were: inlet with a cylindrical flow velocity (Option 1), inlet with zero relative pressure (Option 2), and opening with zero relative pressure (Option 3).

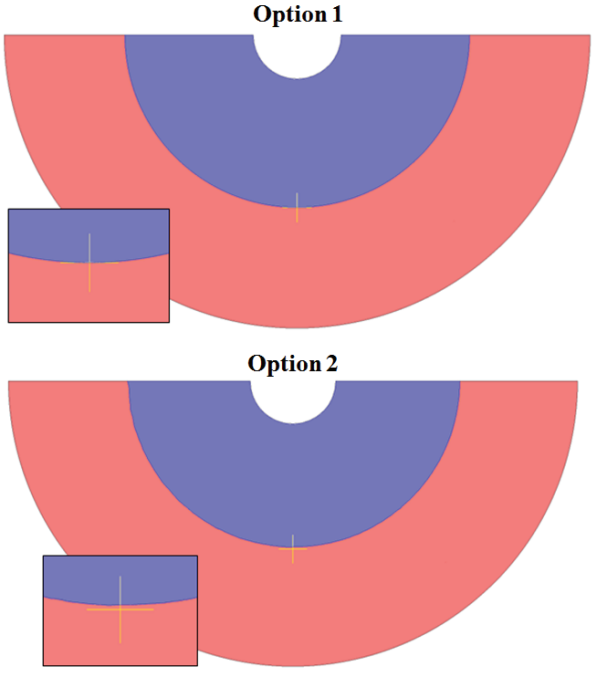

Figure 12: Velocity contour plot of the domain flow field at a rotational velocity of 1.312×10^{-1} radians/s, *Option 1* (top) and *Option 2* (bottom). The boundary line between the red and blue contours represents the flow where the linear velocity is 1.543m s^{-1}, while the yellow crosshair represents the intended location of the SUBOFF centre of buoyancy

Option 1 was found to produce an accurate and uniform angular flow field, with a linear velocity error of less than 0.01% of the theoretical solution at *CB*. Option 2 was found to have slight non-uniformity at the Inlet and a less accurate flow field throughout the domain with an error of about 1.5% at *CB*. To illustrate the findings, Figure 12 shows a velocity contour plot of the flow field for *Option 1* and *Option 2*. The boundary line between the red and blue contours represents the flow where the linear velocity is 1.543m s^{-1}, while the yellow crosshair represents the location of *CB*. Option 3 was found inadequate for the current work as the flow field produced was non-uniform throughout the fluid domain (see Figure 13). The verification was carried out using both turbulence models, BSLRSM and SSTCC. The results for BSLRSM and SSTCC were found to be identical.

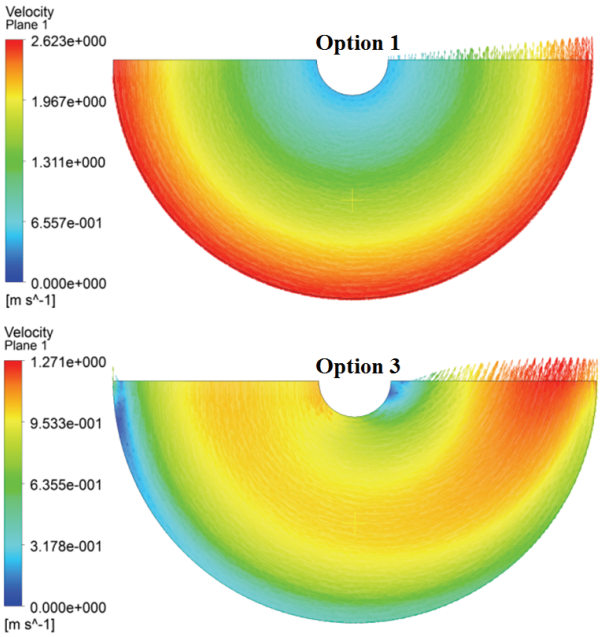

Figure 13: Velocity contour plot of the domain flow field with flow vectors superimposed at a rotational velocity of 1.312×10^{-1} radians/s, *Option 1* (top) and *Option 3* (bottom)

4.3 DISCRETISATION STUDY

4.3 (a) Mesh Independence Study

Figure 14 shows the predicted forces and moments as a function of mesh density at a drift angle of 16 degrees. It is seen that at about 4 million elements the longitudinal force, lateral force and yawing moment predictions of the BSLRSM and SSTCC were within 1.2% of the finest mesh investigated. As a conservative measure the 5.7 million elements mesh model configuration was used for the remainder of the rotating arm manoeuvre study.

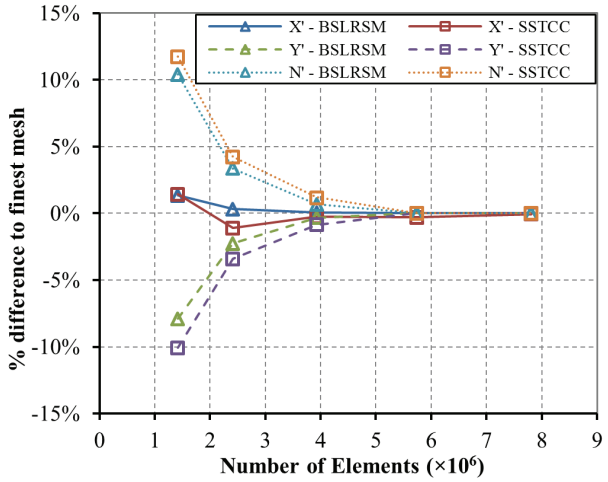

Figure 14: Percentage difference of the longitudinal force coefficient *X'*, lateral force coefficient *Y'* and yawing moment coefficient *N'* predictions from the finest 7.8 million elements mesh solution vs number of mesh elements for the SUBOFF rotating arm manoeuvre test case at a drift angle of 16°

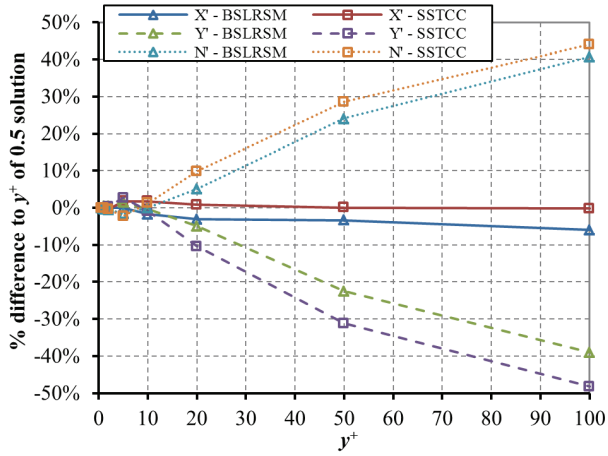

Figure 15: Percentage difference of the longitudinal force coefficient *X'*, lateral force coefficient *Y'* and yawing moment coefficient *N'* predictions as percentage difference from the y^+ of 0.5 solution versus y^+ for the SUBOFF rotating arm manoeuvre test case at a drift angle of 16°

4.3 (b) y^+ Study

Figure 15 shows predicted forces and moments on the SUBOFF model with respect to the mean y^+ around the hull at a drift angle of 16 degrees. Using the solution at y^+=0.5 as the baseline; it was observed that the longitudinal force, and lateral force and yawing moment predictions were consistent with less than 0.5% variation at $y^+ \leq 2$ for the both the BSLRSM and SSTCC. At $2 < y^+ \leq 100$, the longitudinal predictions of the BSLRSM and SSTCC model were found to be fairly consistent with less than 6.0% variation throughout the y^+ range. The lateral force and yawing moment predictions were found to be highly sensitive to y^+ as it increased above 5. The lateral force predictions were found to decrease as y^+ increases, with variations up to 39.0% for the BSLRSM and 44% for the SSTCC model at y^+=100.

The results above show that the longitudinal force, lateral force, and the yawing moment predictions are consistent (within 0.5%) at y^+ of 2 and below. Therefore, a y^+ of 0.5 was selected for the mesh model to be used in the full set of rotational simulations, ensuring that the maximum y^+ value of the first wall node height falls well below a y^+ of 1. The reasons for the trends observed above, and consequently the conclusions drawn, are similar to those discussed previously for the straight-line manoeuvre mesh study.

4.3 COMPARISON WITH EXPERIMENTS

Figure 16 shows the predicted forces and moments on the SUBOFF undergoing rotating arm manoeuvres at different drift angles in comparison with the experimental data by Toxopeus et al. [14]. The uncertainty in the experimental longitudinal force, lateral force and yawing moment measurements were 8.1%, 4.9% and 4.1%, respectively [14]. The influence of the mounting arrangement on the measured forces and moments in the experiment was reported to be about ±5%, thus the overall experimental uncertainty for *X'*, *Y'* and *N'* amounts to 13.1%, 9.9%, and 9.1%, respectively.

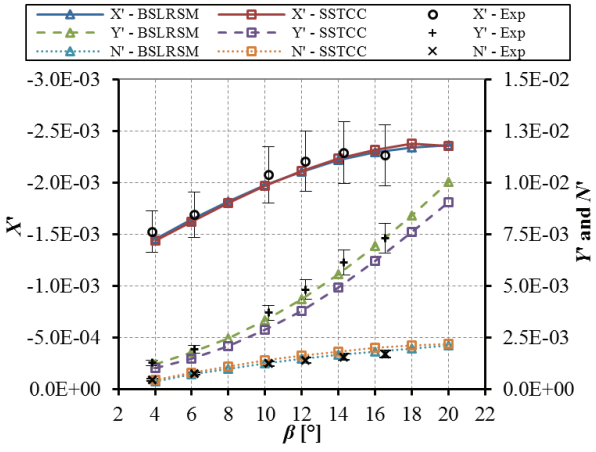

Figure 16: CFD predictions and experimental measurements [14] of the longitudinal force coefficient *X'*, lateral force coefficient *Y'*, and yawing moment coefficient *N'* versus drift angle for the SUBOFF rotating arm manoeuvre test cases. Error bars represent the uncertainty of the experimental measurements

The longitudinal force predictions of the BSLRSM and SSTCC were found to be well within 4.8% and 5.8% of the experimental measurements respectively. The lateral force predictions of the BSLRSM were in good agreement with experimental data and within the experimental uncertainty limit. However, the SSTCC model under-predicted the lateral force by up to 22.4%, which was well

outside the 9.9% experimental uncertainty, although it still captured the general trend in the lateral force measurements. The yawing moment was reasonably well captured by both turbulence models, with BSLRSM in closer agreement with experimental data compared to the SSTCC. The BSLRSM predictions were within the 9.1% experimental uncertainty, while the SSTCC was found to over-predict the yawing moment by up to 16.4% at drift angles above 4°.

The above findings clearly show the superior performance of the BSLRSM compared to the SSTCC in predicting the hydrodynamic coefficients of the SUBOFF undergoing the rotating arm manoeuvre at different drift angles, and are consistent with the findings from the straight-line manoeuvre test case.

5. CONCLUSION

In order to obtain hydrodynamic coefficients of underwater vehicles, RANS-based CFD simulations of the unappended SUBOFF geometry undergoing straight-line and rotating arm manoeuvres at different drift angles were conducted. This included the selection of the appropriate turbulence models together with the required mesh conditions, including the selection of the first and total inflation layer thickness, and the appropriate simulation settings. The study investigated both the BSLRSM and SSTCC turbulence models for both manoeuvring cases in comparison to experimental measurements. It was shown that with the proper setting the BSLRSM predictions offers good agreement with the experimental measurements for both the straight-line and rotating arm manoeuvre test cases.

The SSTCC model is able to satisfactorily predict the longitudinal forces; however, it tends to under-predict the lateral force, and to over-predict the yaw moments in the straight-line and rotating arm test cases well outside the experimental uncertainty limits. This suggests that the SSTCC model is inadequate for the purpose of determining the hydrodynamic coefficients of hull forms similar to the SUBOFF geometry, while the BSLRSM with the correct settings is well suited for such simulations. Although the BSLRSM was found to be 20% longer in computational time compared to the SSTCC, the accuracy gained by using the BSLRSM is shown to outweigh the extra computational time. For future work, it is desirable to gain more insight into what causes the difference in performance between the BSLRSM and SSTCC. The authors believe the difference is due to the sensitivity of the model to adverse pressure gradient in the boundary layer.

The study also examined the effects of boundary conditions and mesh quality on the predictions, leading to the following conclusions for the turbulence models used:

- The flow field quality of the fluid domain in the rotational motion test case was found to be highly sensitive to the boundary conditions, in particular the inlet condition. Thus, it is essential to verify the flow field before carrying out simulations with the vehicle within the domain.
- When using the low Reynolds wall treatment model, an initial y^+ of 0.5 is recommended to ensure the y^+ stays below 1 throughout the surface of the vehicle. The force and moment predictions showed high level of variation as y^+ increased above the threshold of 2.
- The wall function was found to be inadequate for the investigation of the SUBOFF at high drift angles. Variations in the force and moment predictions of up to 10% was observed at around the y^+ of 10 when compared to the low Reynolds wall treatment solution at y^+ of 0.5.
- If the wall function is used due to resource restrictions, then a y^+ near the minimum limit of 10 is recommended as the quality of the lateral predictions using the wall function is shown to depreciate significantly as y+ increases beyond this value.
- For an unstructured hybrid tetrahedral mesh, it is strongly recommended that the minimum total thickness of the layers is equal to at least 1.5 times Prandtl's $1/7^{th}$ power law estimate of a turbulent boundary layer thickness over the surface length of the vehicle, i.e. $1.5\times0.16L_S/\mathrm{Re}_{L_S}^{1/7}$. Under-prescribing the total thickness resulted in higher longitudinal force predictions and lower lateral force predictions compared to the recommended thickness, while over-prescribing the total thickness showed no noticeable differences in prediction.

The promising results of the BSLRSM based on the CFD methodology above will be extended to the upcoming work on multiple underwater vehicles operating in close proximity. However, it will be important in future work to assess and validate the ability of BSLRSM to predict hydrodynamic interaction between the vehicles in relative motion given the numerous modelling factors that can influence its accuracy. Notwithstanding the minimising of all uncertainties, if discrepancy in accuracy of the BSLRSM compared to the validation data persist, a comprehensive transient-based turbulence models such as Large Eddy Simulation (LES) or hybrid RANS-LES maybe required.

6. REFERENCES

1. ALIN, N., BENSOW, R. E., FUREBY, C., HUUVA, T., and SVENNBERG, U., Current Capabilities of DES and LES for submarines at straight course, *Journal of Ship Research*, *Volume 54*, *pp 184-196*, 2010.
2. FELL, B., *Structured Mesh Optimisation of the Fully Appended DARPA SUBOFF Model*, BEng Thesis, Australian Maritime College, 2009.
3. ACKERMANN, S., RANMUTHUGALA, S.D., WIDJAJA, R., and ANDERSON, B., Computational Fluid Dynamics of Suboff Submarine with Sail and Stern Appendages,

Proceedings of the Pacific Underwater Defense Technology Conference, Sydney, Australia, 2008.

4. DUDA, B.M., MENTER, F.R., HANSEN, T., and ESTEVE, M-J., Scale-adaptive simulation of a hot jet in cross flow, *Journal of Physics: Conference Series, Volume 318*, *pp 1-6*, 2011.
5. FELDMAND, J., *DTNSRDC Revised Standard Submarine Equations of Motion*, David Taylor Naval Ship Research and Development Center, Maryland, 1979.
6. GROVES, N., HUANG, T., and CHANG, M., *Geometric Characteristics of DARPA SUBOFF Models (DTRC Models Nos. 5470 and 5471)*, David Taylor Research Center, Maryland, 1989.
7. KIM, S.E., RHEE, B.J., and MILLER, R.W., Anatomy of turbulent flow around DARPA SUBOFF body in a turning manoeuvre using high-fidelity RANS computations, *International Ship Building Progress*, *Volume 60*, *pp 207-231*, 2013.
8. MARSHALLSAY, P.G., and ERIKSSON, A.M., Use of computational fluid dynamics as a tool to assess the hydrodynamic performance of a submarine, *Proceedings of the 18th Australasian Fluid Mechanics Conference, Australia, pp 1-4*, 2012.
9. MENTER, F.R., Trends and challenges in modelling complex turbulent flows, *Proceedings of the 14th International Conference on Fluid Flow Technologies, Hungary*, *pp 1-10,* 2009.
10. PHILLIPS, A.B., TURNOCK, S.R., and FURLONG, M., Influence of turbulence closure models on the vortical flow field around a submarine body undergoing steady drift, *Journal of Marine Science and Technology*, *Volume 15*, *pp 201-217*, 2010.
11. RODDY, R.F., *Investigation of the Stability and Control Characteristics of Several Configurations of the DARPA SUBOFF Model (DTRC Model 5470) from Captive-Model Experiments*, David Taylor Research Center, Maryland, 1990.
12. SMIRNOV, P.E., & MENTER, F.R., Sensitization of the SST Turbulence Model to Rotation and Curvature by Applying the Spalart-Shur Correction Term, *Journal of Turbomachinary*, *Volume 131*, *pp 1-8*, 2009.
13. TOXOPEUS, S., Viscous-flow calculations for bare hull DARPA SUBOFF submarine at incidence, *International Shipbuilding Progress*, *Volume 55*, *pp 227-251*, 2008.
14. TOXOPEUS, S., ATSAVAPRANEE, P., WOLF, E., DAUM, S., PATTENDEN, R., WIDJAJA, R., ZHANG, J.T., and GERBER, A., Collaborative CFD exercise for a submarine in a steady turn, *Proceedings of ASME 31st International Conference on Ocean, Offshore and Arctic Engineering, Brazil*, *pp 761-772*, 2012.
15. VAZ, G., TOXOPEUS, S., and HOLMES, S., Calculation of manoeuvring forces on submarines using two viscous-flow solvers, *Proceedings of ASME 29st International Conference on Ocean, Offshore and Arctic Engineering, China*, *pp 1-13*, 2010.
16. WATT, G.D., BAKER, C.R., and GERBER, A.G., *ANSYS CFX-10 RANS normal force predictions for the series model 4621 unappended axisymmetric submarine hull in translation*, Defence Research and Development Canada, Ottawa, 2006.
17. WHITE, F.M., *Fluid Mechanics*, 5th Ed, McGraw-Hill, New York, 2003.
18. ZENG, G.H., and ZHU, J., Study on key techniques of submarine manoeuvring hydrodynamics prediction using numerical method, *Proceedings of Second International Conference on Computer Modeling and Simulation*, China*, pp 83-87*, 2010.
19. ZHANG, J.T., MAXWELL, J.A., GERBER, A.G., HOLLOWAY, A.G.L., and WATT, G.D., Simulation of the flow over axisymmetric submarine hulls in steady turning, *Ocean Engineering*, *Volume 57*, *pp 180-196*, 2013.

